

Competitive Seeded Growth: An Original Tool to Investigate Anisotropic Gold Nanoparticle Growth Mechanism

Z. Cansu Canbek Ozdil, Olivier Spalla, Nicolas F Menguy, Fabienne Testard

▶ **To cite this version:**

Z. Cansu Canbek Ozdil, Olivier Spalla, Nicolas F Menguy, Fabienne Testard. Competitive Seeded Growth: An Original Tool to Investigate Anisotropic Gold Nanoparticle Growth Mechanism. Journal of Physical Chemistry C, 2019, 123, pp.25320-25330. 10.1021/acs.jpcc.9b05690 . cea-02305660

HAL Id: cea-02305660

https://cea.hal.science/cea-02305660

Submitted on 4 Oct 2019

HAL is a multi-disciplinary open access archive for the deposit and dissemination of scientific research documents, whether they are published or not. The documents may come from teaching and research institutions in France or abroad, or from public or private research centers.

L'archive ouverte pluridisciplinaire **HAL**, est destinée au dépôt et à la diffusion de documents scientifiques de niveau recherche, publiés ou non, émanant des établissements d'enseignement et de recherche français ou étrangers, des laboratoires publics ou privés.

Competitive Seeded Growth: An Original Tool to Investigate Anisotropic Gold Nanoparticles Growth Mechanism

Z. Cansu Canbek Ozdil,[1,2,3] Olivier Spalla,[1] Nicolas Menguy[2] and Fabienne Testard[1,]*

[1]NIMBE, CEA, CNRS, Université Paris-Saclay, CEA Saclay, 91191 Gif-sur-Yvette Cedex, France

[2]Sorbonne Université, UMR CNRS 7590, MNHN, IRD, Institut de Minéralogie, de Physique des Matériaux et de Cosmochimie, IMPMC, 75005 Paris, France

[3]Current Institution: Computer Engineering Department, Bogazici University, 34342 Istanbul, Turkey

ABSTRACT

The influence of initial seed structure on final nanoparticle geometry has been investigated by an original “competitive approach” using SAXS, UV-Vis Spectroscopy and TEM analysis. Herein by using the seed mediated gold nanoparticle growth, seeds with different size and crystalline structure were synthesized and injected into the same growth media. The seeds were chosen due to their different growth evolution into two different morphologies. CTAB coated single crystalline seeds grow into rod like shapes whereas citrate coated multi-crystalline seeds mainly grow into wheat shape polycrystalline particles with small elongation called nanobeans in coexistence with a large quantity of spheres. When seeds are added into the same growth media for competition, a mixture of the different morphologies is obtained. By controlling the number of added competing seeds in the solution, it was found that the multi-crystalline seeds have a higher growth rate than the single crystalline seeds. This has a direct impact on the final distribution of size and morphologies of the nanoparticles. The consequence is a large tendency towards nanobean and sphere structure formation even when a small number of multi-twinned seeds is added in the solution. This method demonstrates the importance of the nature of defects hidden in the initial seed and proves that these defaults are inherited to the final nanocrystal throughout the growth stage from the beginning of the growth. This competitive seeded growth approach is an easy way to identify the influence of seeds morphologies in synthetic pathway of nanoparticles formation.

1. INTRODUCTION

Anisotropic gold nanostructures have drawn an increasing interest in many different fields, due to their size dependent properties, particularly for optical ones. Some of the interesting applications of such nano-systems can be listed as photo-thermal therapy, chemical sensing, drug delivery and biological imaging.[1–6]

All these applications requires high yield syntheses of nanoparticles with low polydispersity.[7–10] From continuous research over a decade on shape and size selection, synthetic routes for anisotropy have been obtained and are well described.[11–16] The main synthetic pathway to optimize the anisotropy uses the famous seeded growth method based on a separation of nucleation and growth stages.[11,13,17] Yet, its major drawbacks is the pollution by other geometrical shapes coexisting with the final desired morphology. Today, the reason for promoting anisotropic growth is still under debate.[18] Even though various mechanisms of anisotropic growth have been described in the literature, such as surfactant preferential binding directed growth,[11,19,20] specific adsorption of silver ions on certain facets of particle,[12,14,17,21,22] these arguments fails to explain the initial symmetry breaking point.[23,24] The intricacy of the multiple influences from the nature of the seeds and the growth conditions controls the overall mechanism towards anisotropic shape. It is well-known that the shapes of nanoparticles are highly determined by their crystal structures like external facets, crystallinity and reaction of additives,[9,18,19,25,26] however how the nature of the seeds and in particular their internal defects influence the final shapes is difficult to predict.[27] [28] Every facet in a nanocrystal has different atomic distribution and therefore singular properties.[28] As a consequence, the specific adsorption of ligands on some facets is often advanced to explain the difference in growth rate and thus the formation of anisotropy.[12,17] In any cases, this argument fails to explain the initial symmetry

breaking point between the isotropic precursor and the final complex anisotropic particle morphology.[29,30]

In 2010, Hubert et al. have shown that anisotropy in gold nanoparticles is developed after a minimum size of 5 nm but the development of anisotropy below this size is still under debate.[31] Liu et al. have shown that for a given growth solution the nature of the seeds could completely modify the final shape and the internal crystal structure.[21] For a given seed structure the nature of the growth solution can also modify the final shape. We recently identified the conservation of the bulk penta-twinned structure inherited from the isotropic decahedral seeds along the growth[32] while external facets are strongly dependent on the nature of the ligands. Xia et al. have evidence the importance of stacking faults, twinned planes in the orientation of the final shape and structure.[33]

In this context, we have selected two sets of small sized seeds with different crystallinity known to grow towards different shapes when added in a growth media containing cationic surfactant, CTAB (bromide cetyltrimetylammonium), silver salt (to promote anisotropy) and ascorbic acid as mild reducing agent (Figure 1a).

In order to highlight the importance of the initial seed precursor on the orientation towards the final nanoparticle geometry, we propose a (Figure 1b) competitive growth method that includes controlled addition of the two different natured seeds in the same growth media. The observation of their growth rate by Transmission Electronic Microscopy (TEM) and in situ UV-Visible spectroscopy affords for the identification of the seeds with the highest reactivity. This method enables us to discuss the importance of the nature of the defects in the initial seeds and to identify the undesirable morphologies of seeds for a chosen final nanoparticle.

2. MATERIALS AND METHODS

2.1. Materials

Cetyltrimethylammonium bromide (CTAB 99%) was purchased from G-Biosciences. Tetrachloroauric(III) acid (extra pure), silver nitrate (extra pure), sodium borohydride (98%), trisodium citrate and L-ascorbic acid were obtained from Sigma without further purification. All the glassware was cleaned with aqua regia and washed with distilled water before the experiments.

2.2. Methods

2.2.1. Synthesis of Seeds

- Type I Seeds

CTAB capped seeds were prepared through the modification of seed mediated method published by Nikoobakht and El-Sayed.[34] Briefly, the nanoparticles were synthesized by the addition of freshly prepared ice-cold $NaBH_4$ solution (0.1 mL, 0.0264 M) into a solution composed of $HAuCl_4$ (0.025 mL, 0.05 M) and CTAB (4.7 mL, 0.1 M). The mixture was strongly stirred for 2 minutes and kept at 28 °C. The obtained solution with a light brown color is used after 1 hour of its preparation.

- Type II Seeds

Preparation of these seeds was inspired from the work of Murphy et al.[11] The synthesis involves the addition of 0.3 mL of ice-cold 0.01 M $NaBH_4$ into a mixture of 10 mL of 0.25 mM $HAuCl_4$ and 0.25 mM sodium citrate under vigorous stirring at 28 °C. The color of the mixture

immediately turned into orange red. Citrate stabilized seeds were aged for 2 hours prior to their use to ensure the fully decomposition of excess borohydride in the solution and to ensure the reproducibility of the synthesis.

2.2.2. Growth of Seeds

The same growth solution was used for the growth of the different seeds, to see the influence of the initial seed structure on the final nanoparticle size and morphology. Chemical composition of the reference growth solution is given in Table 1.

Variable volumes of as-prepared seed solutions were injected into the given growth solution (120 μL and 60 μL respectively for single Type I or Type II seeds and different volumes described in Table 1 for mixture of seeds). Resulting solutions were gently mixed for 15 seconds and kept at 28 °C without disturbance overnight to ensure that the growth is terminated.

Entire presented kinetic experiments, illustrates the final growth solution before any kind of purification. After termination of growth, the solutions (10 mL) were cleaned from excess reactants by two cycles of centrifugation (8440 g, 40 min) using 15 mL *VWR High Performance Centrifugation Tubes*. After the first step of centrifugation, supernatant was discarded and remaining sediment was re-dispersed in pure water to attain the same final volume of solution (10 mL). Following, the second step of centrifugation nanoparticle solution is concentrated to 1 mL for microscopy observations.

2.2.3. Characterization Techniques

UV-Vis Spectroscopy (UV-Vis)

Absorption spectra of final particles were measured in 1mm- Helma cell by using Shimadzu *UV-2550* UV-Vis Spectrophotometer. Data were analyzed with UV Probe Software. For all kinetic experiments UV-Vis spectra's are recorded with delay of 10 seconds after addition of seeds into the growth solution.

Transmission Electron Microscopy (TEM)

Characterizations of the nanoparticles were performed by transmission electron microscopy (TEM). Low resolution electron observations were carried out by *Philips CM 30* operating at 300 kV. An 8 µL drop of concentrated gold nanoparticle solution was dried on a carbon coated copper grid for a night before TEM analysis. HRTEM observations were achieved using a *JEOL 2100F* microscope equipped with Gatan US4000 CCD Camera operating at 200 kV (installed at IMPMC, Sorbonne Université, Paris) and a JEOL ARM200CF microscope equipped with a Gatan US4000 CCD camera and operating at 80 kV (installed at MPQ, Université de Paris, Paris). Following the protocol described in a former publication of Hubert et al.,[31] a semi-automated numerical treatment based on Image J software is used to extract the two first principal components of the nanoparticles, here the length "L" and the diameter "W" of nanoparticles.

Dynamic Light Scattering (DLS)

The size distribution of isotropic gold nanoparticles was monitored using dynamic light scattering (DLS). Analysis was carried out using a *Zetasizer Nano-ZS (MALVERN Instruments)* at 25°C. The size analysis of seeds was carried out immediately after the preparation of the particles. The volume size distribution, the Z-average diameter (Z-ave) and the polydispersity

index (PdI) were obtained from the autocorrelation function using general purpose mode for all analytes.

Small Angle X-Ray Scattering (SAXS)

Two complementary home-made apparatus with different energies were used to attain the respective q ranges 0.01 $Å^{-1}$ < q < 0.35$Å^{-1}$ for SAXS and 0.02 A^{-1}< q < 3 A^{-1} for WAXS. The X-ray sources (rotating copper anode, λ = 1.542 Å with 2.6 10^6 ph/s for SAXS and molybdenum, λ = 0.712 Å with 9 10^7 ph/s for WAXS) are collimated via an Osmic mirror through two hybrid slits (1x1 mm^2). The scattered beam is collected on a Pilatus3R 200K detector for SAXS or on a Mar 345 image plate for WAXS. The sample to detector distance is calibrated from tetradecanol. The detector counts is normalized into differential cross section with 3 mm Lupolen (I_{max} = 6 cm^{-1}) and 1.5 mm water (I = 0.016 cm^{-1}) after a classical radial averaging procedure[35,36] Samples are measured in 1.5 mm (3 mm) glass capillaries for SAXS (WAXS).

Due to the high CTAB concentration (0.1M), type I seeds are analyzed on the WAXS set-up with Molybdenium source while type II seed can be analysed on the SAXS set-up with copper source. A constant is subtracted to account for the effect of Br fluorescence on the WAXS set-up.

3. RESULTS AND DISCUSSIONS

The competitive method developed in this work is derived from the original seed mediated growth in a solution containing CTAB, $AgNO_3$, $HAuCl_4$ and ascorbic acid.[23, 31, 37, 38] Two different types of seeds with different structure, were injected into the growth solution to monitor their crystal growth with respect to each other. Before the addition of the seed solutions to the

growth media, small sized seeds were characterized with UV-Vis Spectroscopy, DLS, SAXS and HR-TEM.

Typical UV-Vis spectra's of as-prepared seeds belonging to the two families are given in Figure 2a. It is known that gold nanoparticles smaller than 5 nm do not exhibit a clear surface plasmon band in UV-Vis region as in the case of Type I seed.[38–40] Increasing the size of the seeds causes appearance of large absorption band around 500 nm as observed in Type II seeds. Even though this information does not supply quantitative information on the size of the particles, it gives a clear idea about the size range that particles exhibit.

To have an accurate quantitative information on the size distribution of the seeds in solution, Dynamic Light Scattering and Small Angle X-ray Scattering are more valuable techniques. However, for the systems containing large quantity of cationic surfactant as in Type I system, DLS is not convenient due to the coexistence of high concentration of charged micelles with low concentration of gold nanoparticles. Only citrate coated NPs could be characterized by DLS to extract the size distribution (Figure S1).

SAXS diagrams of freshly prepared seed solutions are given in Figure 2b. Associated fits using a Gaussian distribution of spheres (Table 2 for parameters) are shown in the resulting diagram with the size distribution curves obtained for the two different seeds (*Figure 2b, inset*). Two size families are produced, one with smaller size (2±0.4nm) coated by a cationic surfactant (CTAB), and the others with larger sizes (4.8±1.8 nm) coated by an anionic ligand (citrate).

Additionally, crystal structure of different as-prepared seeds has been analyzed by using HRTEM technique down to atomic resolution. To prevent any kind of transformation of particles due to beam damage, high resolution imaging has been performed at 80 kV. Such kind of

attention is important for CATB capped particles that show single crystalline structure at small sizes. For Type I seeds, HRTEM images and FFT analysis reveal that a typical 2.1 nm particle adopt single crystalline (SC) structure with well-defined facets (Figure 3a). For highly symmetrical crystalline material like gold, thermodynamic equilibrium shape of small sized SC seed in vacuum is generally predicted as truncated octahedron by using Wulff condition.[41,42] However, it has been recently demonstrated that Wulff conditions are insufficient to describe the structure when surface and edge are strongly interacting with environment[43] which is the case here in the presence of CTAB. This interaction could explain the stabilization of such small sized SC seeds.

For citrate capped seeds detailed analysis has already been presented in our previous work.[38] To sum-up, those particles contain various twinning planes and stacking faults (Figure 3b). The FFTs corresponding to three adjacent subunits, given in the inset of HRTEM image, are related to a <110> zone axis diffraction pattern. Such kind of five-fold-twinned decahedral nanoparticles, are composed of five subunits with the f.c.c. crystal structure sharing {111} crystallographic faces and oriented along a common <110> direction (Figure 3b).[7,21,29,32,34,38]

3.1. Single Seed Oriented Growth

To adapt the experimental protocol for comparison of growth from individual or competitive seeds, we control the number of seed particles (N_{seed}) added in each experiment.

The as-prepared seed solutions cannot be concentrated without a strong modification of the size distribution. Therefore, the number of seeds in growth media is regulated via volume control of added particles using the density numbers and the radius obtained by SAXS analysis (Table 2). Reference conditions for the number of each seeds in a given volume are summarized in Table 3.

Figure 4a represents the temporal UV-Vis evolution of the absorption spectra, monitored during the growth of CTAB capped seeds (Type I). The classical continuous increase in absorbance of both transverse ($\lambda_{T\text{-}SPR}$) and longitudinal surface plasmon peaks ($\lambda_{L\text{-}SPR}$) are clearly visible.[44] Overall growth of nanoparticles is completed in 15 minutes.

It is already known that CTAB capped seeds (Type I) can produce high yield of nanorods, up to 95%, with traditional growth conditions (given in Table 1).[12,13,17] From TEM and HRTEM (Figure 4b and 4c) images, the production of mainly single crystalline nanorods is confirmed after addition of 120µL of Type I seeds in the growth solution. The (L,W) representation[31] clearly identifies the two branches of isotropic and anisotropic shapes (Figure 4d).

The variation of absorbance as a function of time for both characteristic surface plasmon peaks (at $\lambda_{T\text{-}SPR}$ and $\lambda_{L\text{-}SPR}$) and absorbance at 400 nm (A_{400}) is plotted in Figure 5a. Basically, absorbance increases steadily for all given wavelengths with different rates. The variation of the extinction band at 400 nm being related to the total Au(0) concentration in the sample,[46] it is a direct way to access to the reduction kinetic of the gold ions (Au(I) into Au(0)) in the solution (see Fig 2a in SI). The Au(0) production is quite rapid till 630 seconds with a rate production of $6.8\ 10^{-4}$ mM/s. After termination of the growth (630s), total Au(0) amount is found as 0.368 mM. This traduces a yield of 73.6% in the final solution before purification step. Growth rate of characteristic plasmon peaks ($A_{L\text{-}SPR}$ and $A_{T\text{-}SPR}$) can also be identified by the slope of the initial section of the Absorbance (A) vs time plot, respectively $5.8\ 10^{-4}$ unit/s and $1.7\ 10^{-4}$ unit/s. From this temporal evolution, it can be deduced that $A_{L\text{-}SPR}$ is increasing 3.4 times faster than $A_{T\text{-}SPR}$.

$\lambda_{L\text{-}SPR}$ is more sensitive to the shape of the nanoparticles rather than $\lambda_{T\text{-}SPR}$. It is correlated to the aspect ratio (AR) of the nanorods through the empirical relationship (Equation 1):[46–48]

$$AR = \frac{\lambda_{L-SPR} - 478}{96} \quad (1)$$

Results on temporal evolution of both $\lambda_{L\text{-}SPR}$ and AR, are given in Figure 5b. The $\lambda_{L\text{-}SPR}$ reaches its maxima at about 540 seconds, at the resonance wavelength of 795 nm, achieving relative absorbance of approximately 0.28. As the growth time increases, a significant decrease in $\lambda_{L\text{-}SPR}$ starts to appear after 540 seconds, which is the result of reshaping of gold nanorods into less anisotropic nanoparticles with time.

Therefore reshaping occurs close to the completion of the reduction of Au(I) into Au(0). Such trend of reshaping is often observed in classical wet seed mediated growth synthesis of nanorods and generally explained by etching at the tips of nanorods.[49–51]

Initially formed seeds start to elongate rapidly and reaches the aspect ratio of 3.25 in the first 360 second of the reaction. After fast growth stage, increase of AR continues with slow speed followed by steady decrease. In this stage nanorods rearrange their aspect ratios to lower values. This final stage of gold nanorod growth is followed by the stabilization of AR. This tendency is in perfect agreement with the results obtained by Becker et al.[52] where maximum aspect ratio is attained around 360 s for similar chemical conditions.

With Type II seeds, another morphology is obtained as described by Liu et al.[21] Bipyramids or nanograins with internal defects[32] are produced. Figure 6a represents the absorbance plot of the growth solution after addition of 60 μL Type II seeds. As in the previous case, two distinct plasmon bands are visible similar to the ones observed for nanorods. Mainly, the difference between spectra is that, for nanobeans, the absorbance value for $\lambda_{L\text{-}SPR}$ is lower than for $\lambda_{T\text{-}SPR}$. This results from high yield of isotropic nanoparticles simultaneously formed during the growth of anisotropic nanobeans (Figure 6b-d) for these chosen growth conditions.

From the absorbance values at 400 nm represented in Figure 7a, (Figure S2-b), one can found that the concentration of gold attain a limit of 0.320 mM after 1350s. By the end of the reaction, 67.2% of initial ionic gold is reduced. Contrary to nanorods case, the blue shift of the plasmon band starts long before the completion of the reduction of Au(I) into Au(0). This blue shift is the signature of change in the gold reduction on given facets and reshaping, as it continues after the completion of the reduction.

Because the $\lambda_{T\text{-}SPR}$ signal is the result of the superposition of two different signals (*from high yield spherical nanoparticles and nanobeans*), no straight forward information on the growth rate of different morphologies, by using slope of the Absorbance(t) $A_{T\text{-}SPR}(t)$ curve, can be deduced. Plot of the evolution of $\lambda_{L\text{-}SPR}$ with time indicates a red shift from 678 nm to 750 nm in the early stages of growth (Figure 7b). After reaching its maximum value (765 nm), a strong decrease is observed down to 660 nm after 30 minutes.

Kinetic of conversion of Au(I) into Au(0) for both nanorods (Figure 5a and Figure S2-a) and the bean shape nanoparticles (Figure 7a and Figure S2-b) can be compared from the slope of the Absorbance $A_{400nm}(t)$. For nanorods, the absorbance at 400 nm is increasing about nearly 2 times faster than for nanobeans ($1.7\ 10^{-4}$ Vs $9.1\ 10^{-5}$ unit/s). This means that the rate of ionic gold conversion is slower for the nanobeans solution. The reason can simply be explained by the lower numbers of Type II seed ($1.8\ 10^{12}$) added in comparison to Type I seed ($5.52\ 10^{13}$). In seeded growth method it has been proved that the Au(I) to Au(0) transformation proceeds through surface catalyzed reduction.[36] The transformation is thus favored by a larger available surface of gold seed ($6.9\ 10^{14}$ nm^2 for Type I seed against $1.3\ 10^{14}$ nm^2 for Type II seeds). However for comparison, the rate of Au(0) production per seeds has to be considered, it is found

that the rate is 17 times higher for Type II seed than for Type I seed. This indicates a higher reactivity for MTW citrate capped seeds than for SC CTAB capped seeds.

From the comparison of the growth from two different kinds of seeds in a given CTAB/$AgNO_3$/AA growth solution, we retrieve that the final state is controlled by the seed's morphology and that the defects in the seeds are crucial in the orientation of the final structure.[33]

3.2. Revealing the Kinetics of Simultaneous Growth Between Two Type of Seeds

To measure the relative rate of growth between different seed structures, we have adapted a competitive growth technique. As indicated previously, the competitive method includes the addition of two seeds, prepared with different methods, into the same growth solution. In contrary to the single seed growth (Figure 1a), in the competitive growth system, both seeds will compete for the same gold source in a surfactant rich medium (Figure 1b).

Table 4 summarizes the set of competitive experiments performed with different seed volumes, V_α (*V_1 corresponding to the volume of Type I seed and V_2 to Type II seed)*. In the table, N_α represents the total number of each seeds in the corresponding volume. The balance between the two seeds family is given by the number percentage of each seed ($\% N_\alpha$) and the related surface area percent ($\% \Sigma_\alpha$). For the 3 experimental conditions described in Table 4, the number of Type I seed (N_1) is always higher than the number of Type II seeds (N_2).

It is clearly visible from the TEM images given in Figure 8 (a-c) that with increasing number of Type II seeds, the ratio of nanorods strongly decreases in favor of spherical and nanobeans shapes. It is more evident with the *(L,W)* plot in Figure 8 (d-f)[31] obtained from about 900 nanoparticles to identify the different morphologies. In the three conditions, two different

populations (isotropic and anisotropic shapes) are clearly visible; with distinct variation in their proportion.

In the first sample (S1), in which seeds are composed of 99% of Type I seed (77 times more seeds I than seeds II), most of the population is occupied by nanorods (82%) with small number of elongated nanobeans (7%) and spherical particles 11%. Large nanorod population prevents to visualize the nanobeans in the *(L,W)* plot since both populations are superimposed (Fig. 8d).

For the case S2, where the relative number of Type II seeds is increased from 1.3% to 6.2% (15.5 times more seed I than seeds II), TEM images (Figure 8b) shows that, even though the nanorods keep their structure, bipyramids are formed. In this case, *(L,W)* plot, given in Figure 8e, shows that both nanorods and bipyramids lay on the same line with an average aspect ratio of 3. This is probably due to existence of excess monomer in the environment promoting the growth of both types of seeds. It is clear that the population of nanorods decreases, with respect to S1, from 82% to 53% while the bipyramidal particles increase their number (13%) as well as the spherical nanoparticles (34%). For these two cases, there is also a large amount of small sized particles (below 15 nm) located between the two branches (isoptropic and anisotropic) of the distribution in comparison to the single added seeds as given in Figure 4d and Figure 6d for Type I and Type II seeds respectively[53] (see also figure S4 where the 5 cases are plotted on a single figure).

For the last sample indicated as S3, TEM results, given in Figure 8c, shows slight number of nanorods (20%) and high concentration of bean shape nanoparticles (42%) coupled with spherical shapes (38%). This means that, due to further increase of the number of Type II seeds to 11.5%, the population of the nanorods decreases to a critical point even though the number of seed I is 7.6 larger than number of seed II. Also, no bipyramidal shapes (*i.e. with sharp tips*) are

observed on this type of samples. For this case, (L,W) plot (fig 8f) is similar to the one obtained from single Type II seed (Figure 6d) with an added small population of nanorods. (see fig S4 where the 5 cases are plotted on a single figure).

To sum up, when the number percentage of Type I seeds is higher than 98 %, high amount of nanorods are obtained, whereas slight number of nanobeans are formed due to the low amount of Type II seeds. As soon as the number of Type II is increased to 6%, the proportion of nanobeans/bipyramids and spherical particle increases with respect to the nanorods even though the growth solution includes large number of Type I seeds.

By these results, we can conclude that the reduction of Au(I) to Au(0) is favored primarily on the surface of Type II seeds (citrate seeds) rather than Type I. The higher transformation rate per seed of seed II (17 times higher than for seed I) limits the production of nanorods in case of competitive growth. The favored Type II seeds, consume most of the available Au(I) during the growth and starts to promote the formation of bipyramids. This is supported by the presence of high population of low AR of nanorods and small sized spherical nanoparticles in the (*L,W)* plot when initial seed contains 94% of Type I seed and 6% of Type II seed (ratio 15,5 between seed I and seed II) (Fig 8e). The reason of such preferential growth, may be explained by the presence of large numbers of twinning planes and highly reactive edges on the surfaces of Type II seeds.[7] For a given growth condition, the initial structure of the seed is a key parameter to control the final shapes. Further increase in the number percentage of Type II seeds to 11.5%, increases the active surface area of these type of seeds from 28% to 44% and decreases the one for Type I seeds from 72% to 56%. In this case, only favored Type II seeds grow into nanobeans with few chance for Type I seeds to form the nanorods.

This competitive growth permits to explain why the yield of nanorods is never 100% for single growth from CTAB capped seeds. Namely, these type of seeds are in majority monocrystalline, but they also contain a few proportions of multi-twinned seeds (*similar to Type II seed*). This creates a situation, resembling to the competitive growth conditions, like a fast consumption of gold monomer by the slight number of polycrystalline seeds to produce either spherical shapes or nanobeans as side products during synthesis of gold nanorods. This is even worse for aged CTAB seed solution where the proportion of MTW particles is increasing. The yield of SC gold nanorods decreases with the increasing time aging of the CTAB seed solution as shown by Park et al.

The temporal evolution of the UV-Vis spectrum, given in Figure 9, corresponds to the conditions of case S2. With these synthesis conditions, we observe difficulties on controlling the yield and the AR of the bipyramids which is directly related to the position and the intensity of $\lambda_{L\text{-}SPR\ (2)}$. Such control of AR in multi-twinned NPs is even harder when the initial pH is not imposed during the growth (see Figure S5). Namely, when pH is not well controlled, chloride ions and dissolved oxygen, present in the solution, leads to strong etching on the tips of the nanobeans or the bipyramids to transform the morphology into thermodynamically stable spherical shapes. Such morphological transformations are at the origin of the shift of $\lambda_{L\text{-}SPR}$ (*both for nanobeans and bipyramids*) to lower wavelengths.[14,54,55]

The evolution of absorbance in time is presented for $A_{T\text{-}SPR}$, $A_{L\text{-}SPR(1)}$ and $A_{L\text{-}SPR\ (2)}$ in Figure 10a for the spectrum given in figure 9. For $A_{T\text{-}SPR}$ the continuous increase stops around 1170 seconds reaching to a saturation point in absorbance at 0.132. Decrease of the absorbance in longitudinal modes ($A_{L\text{-}SPR(1)}$ and $A_{L\text{-}SPR(2)}$) after 450 second can be attributed to the separation of the superposition of both signals, removing the contribution from each other. The number of final

colloidal gold concentration integrated in nanoparticles at the end of the reaction is found as 0.35 mM (by using the final absorbance value obtained at 400 nm after termination of the reaction in 30 minutes), this corresponds to 70% yield of transformation.

The temporal evolution of each characteristics plasmon peaks is given in Figure 10b. A single $\lambda_{L\text{-}SPR}$ is visible in the early stages with the associated wavelength evolving from 710 nm to 760 nm. After 350 seconds, with the separation of the large signal of nanobeans, plasmon band of nanorods ($\lambda_{L\text{-}SPR\ (1)}$), becomes visible at 760 nm and remains at constant position meaning that nanorod growth is completed below 350 seconds (Figure 10b). In comparison to the 700s observed for the single seed I oriented growth, the final state is attained at a shorter time. This has to be related to the depletion of monomers during the growth stages, while both Type I seeds and Type II seeds are growing in competition from the same Au(I) solution. The broad signal of nanobeans $\lambda_{L\text{-}SPR\ (2)}$, starting at 721 nm shows a strong decrease to lower wavelengths, to finally merge with $\lambda_{T\text{-}SPR}$ around 583 nm due to the reshaping. The growth rates found for $A_{L\text{-}SPR}$ and A_{400nm} are in perfect agreement with the expected values issued from the proportion of added seeds and growth rate per seed, respectively 4.4 10^{-4} unit/s and 2.0 10^{-4} unit/s (for expected 4.2 10^{-4} unit/s and 1.8 10^{-4} unit/s).

To conclude, given longitudinal plasmon peaks, appearing at the early stage of growth, corresponding to the two modes for the two different anisotropic structures; one being for nanorods ($\lambda_{L\text{-}SPR\ (1)}$) and the other for bipyramids ($\lambda_{L\text{-}SPR\ (2)}$) do not show the same stability against reshaping. Mainly, in competitive experiments the different seeds grow independently form each other from the very beginning of the reaction.

4. CONCLUSION

Even though there has been much progress in the synthesis of anisotropic gold nanoparticles, the control of seed structure for the selection of final geometry remained as a key factor to understand the formation mechanism. Here, from an original competitive seeded growth method we are able to identify the strong difference in reactivity between two seeds families. Namely, by combining TEM and time resolved UV-Vis Spectroscopy, the formation of anisotropic gold nanoparticles obtained by a combined addition of two as-prepared seeds (single crystal or multi-twinned) has been investigated. When nanoparticles smaller than 5 nm competes for the same gold source, the partition between two unique anisotropic structures (single crystal nanorods and multi-twinned bipyramids/beans) is observed. The final morphology of nanoparticles depends strongly on the initial mixture of seeds morphologies. Mixing single crystalline seeds (Type I), known to produce single crystalline nanorods plus spherical particles and decahedral seeds (Type II), known to produce nanobeans/bipyramids and also spherical particles, leads to a mixture between all listed morphologies. By imposing the number percentage of the two seeds (Type I/Type II), it was shown that individual seeds continue their growth separately in the same reaction container, even though growth kinetics for both morphologies differs from each other. We demonstrate that the surface area of the seeds and the growth rate per seeds are important parameters to rationalize the proportion of the obtained anisotropic NPs.

Increasing the fraction of the multi-twinned seeds causes a rise in the number of the final anisotropic NP that it is responsible for. Even added in a low proportion, the added seeds have a strong impact on the final distribution. This is a direct consequence of the large difference between the growth rates of the competing seeds, with a higher growth rate for the MTW seeds. The competitive method is thus an indirect way to evaluate the ability for a seed to grow.

The competitive growth exhibits the importance of defects hidden in the initial seeds and how the final crystal defects could be inherited from seeds during the growth stages. It is an original way to identify the undesirable seeds morphology for a chosen final structure. Beyond the mechanistic tools offered by this methodology, these results have to be related to the difficulties in controlling defects in small size nanoparticles and the necessity for developing analytical tools for a complete determination of nanoparticles' shape, size, and crystallinity at the atomic scale [56]. The competitive approach can be used as an efficient tool to understand the mechanism of growth for various types of complexe structures and materials. In addition, it offers a tool to explore competitive growth in real material.

FIGURES

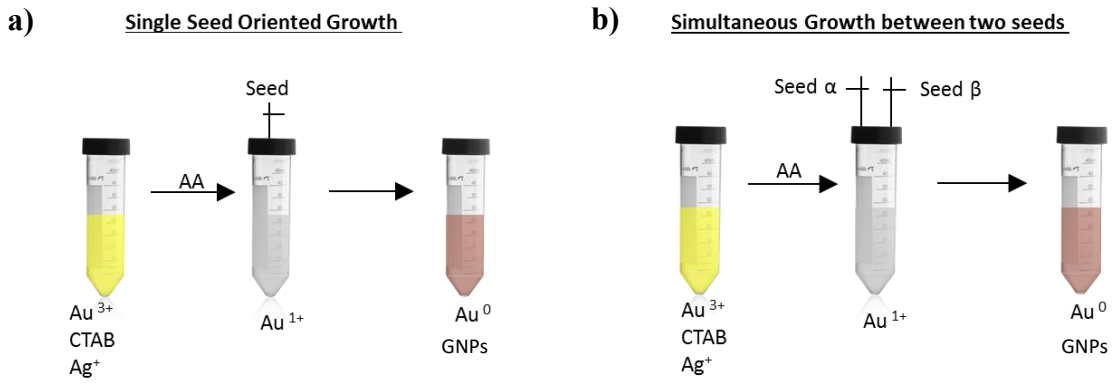


Figure 1. Generation of gold nanoparticles via seed mediated synthesis of a) single seed oriented growth b) competitive growth

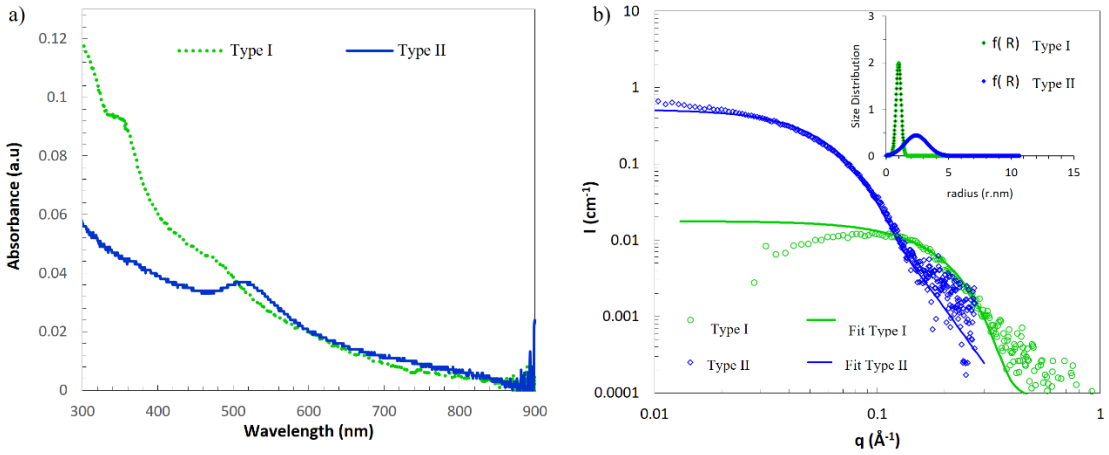


Figure 2. (a) UV-Vis Spectrum of as-prepared seeds from different methods (b) SAXS patterns of Type I and Type II seeds. Lines correspond to the theoretical curves obtained by fitting with a Gaussian distribution of spheres (parameters are given in table 2). Distribution curves obtained are given in the inset of the figure

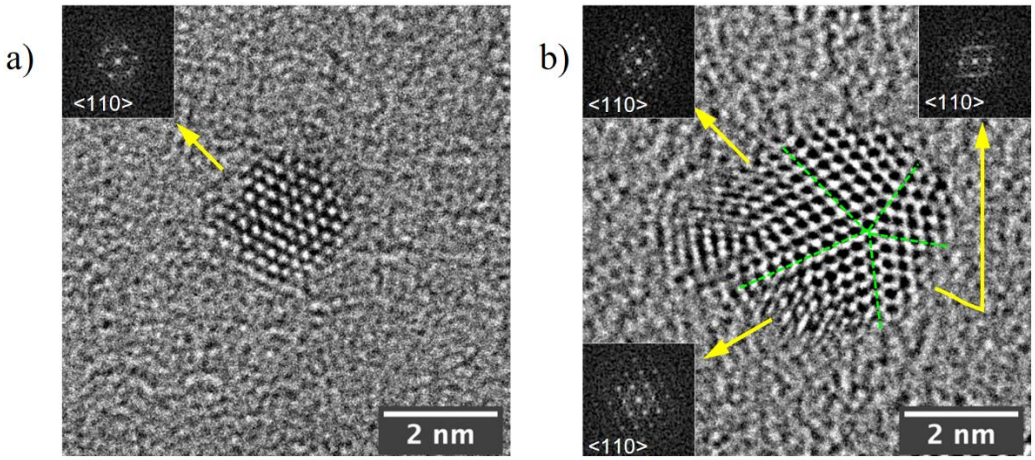


Figure 3. HRTEM images of (a) CTAB capped seeds - Type I and (b) Citrate Capped Seeds - Type II. Insets correspond to FFT related to area indicated by yellow arrows. The dashed green

lines in (b) are a guide for the eye indicating the twinning planes between each sub-unit of the decahedral particle.

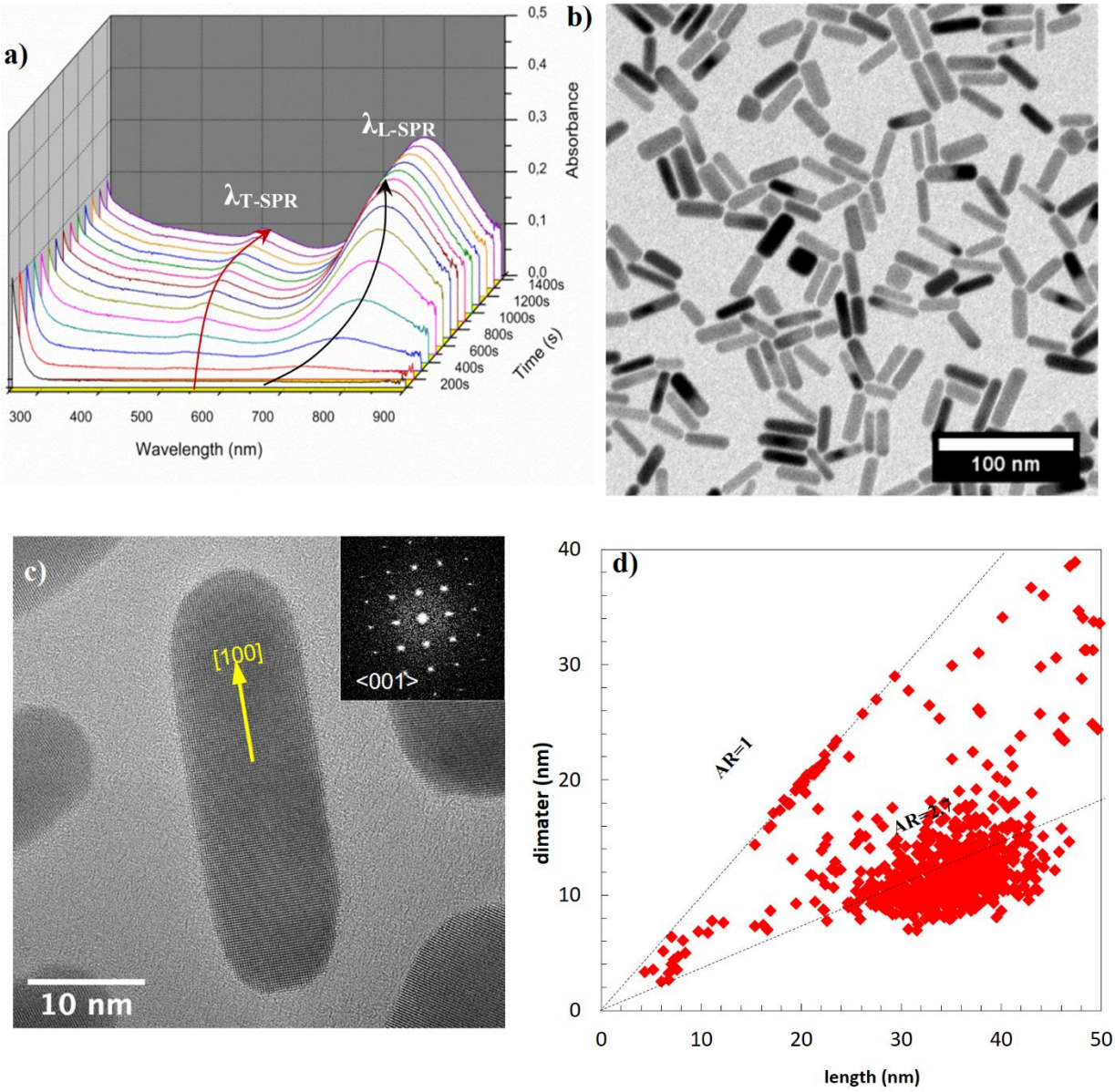


Figure 4. (a) UV-Vis Spectrum of growth solution after addition of 120 µL of Type 1 seed in growth solution (*spectra's are recorded with delay of 10 s starting from the moment of addition of seeds into growth media)* (b) TEM image of final nanoparticles after termination of the growth

(c) HRTEM image of single nanorod oriented along [001] axis (d) Size analysis of sample obtained from TEM images (one of them is given in b)

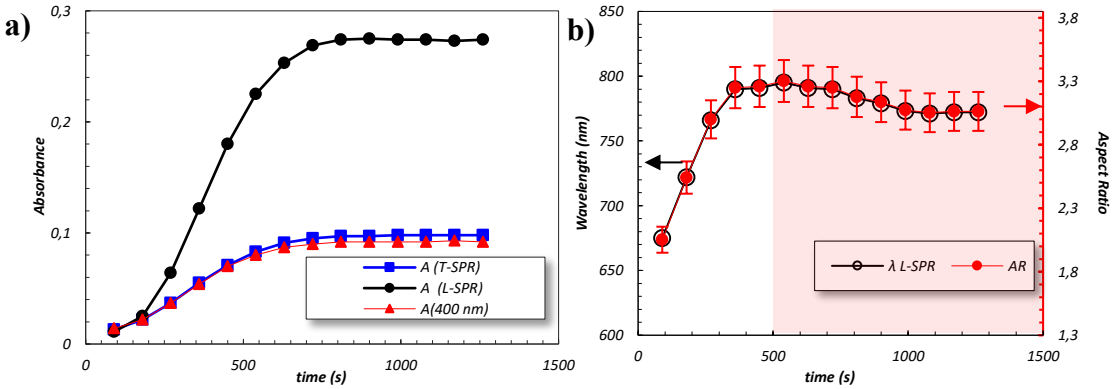


Figure 5. (a) Evolution of absorbance for longitudinal, transverse LSPR and at 400 nm with time (b) evolution of localized plasmon resonance wavelength and aspect ratio (AR) with time

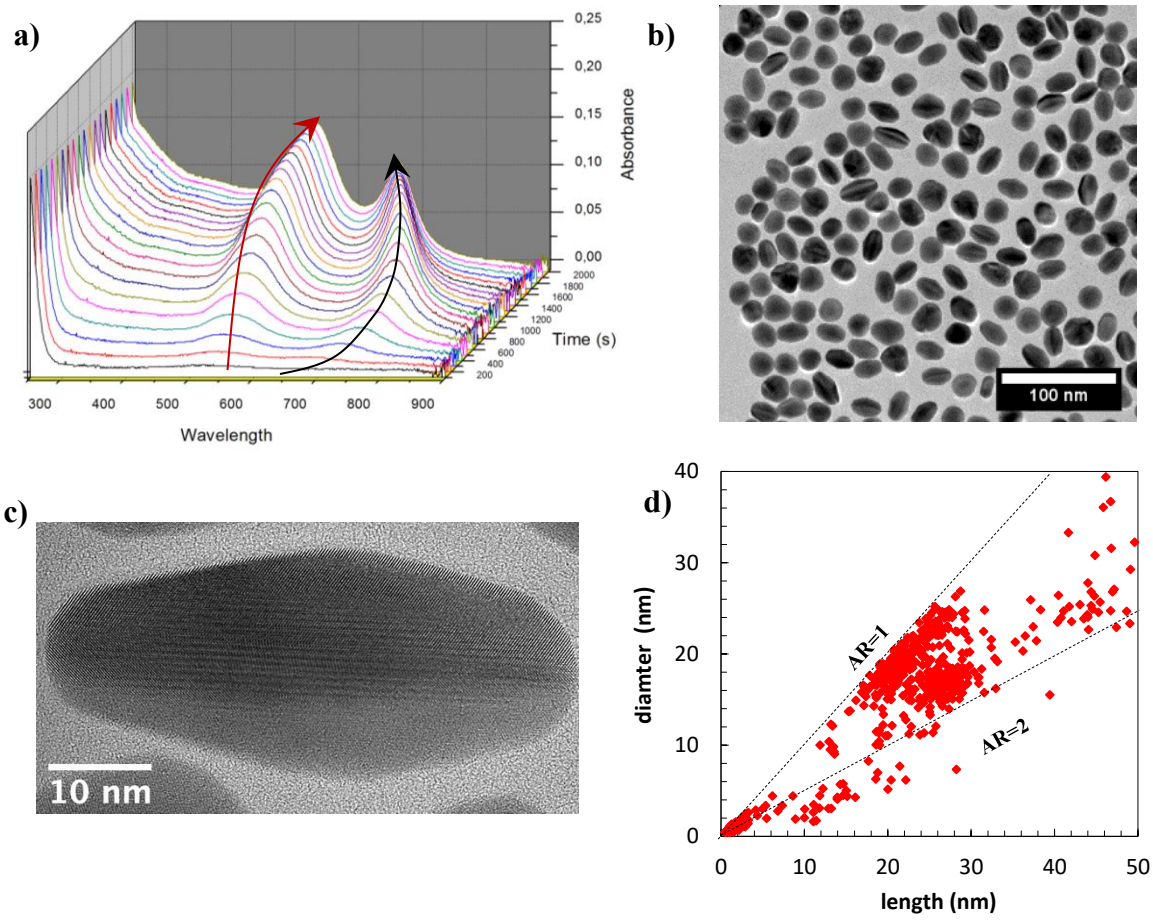


Figure 6. (a) UV-Vis Spectrum of growth solution 10 seconds after addition of 60 µL of Type II seed in growth solution (b) TEM image of final nanoparticles after termination of the growth (c) HRTEM image of single bipyramid (d) Size analysis of sample obtained from TEM data

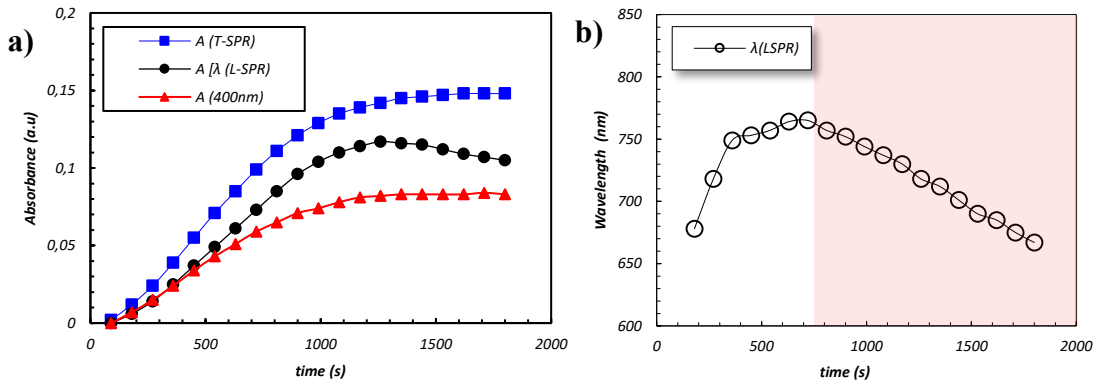


Figure 7. a) Evolution of absorbance for longitudinal, transverse LSPR and at 400 nm with time (b) evolution of longitudinal surface plasmon resonance wavelength with time

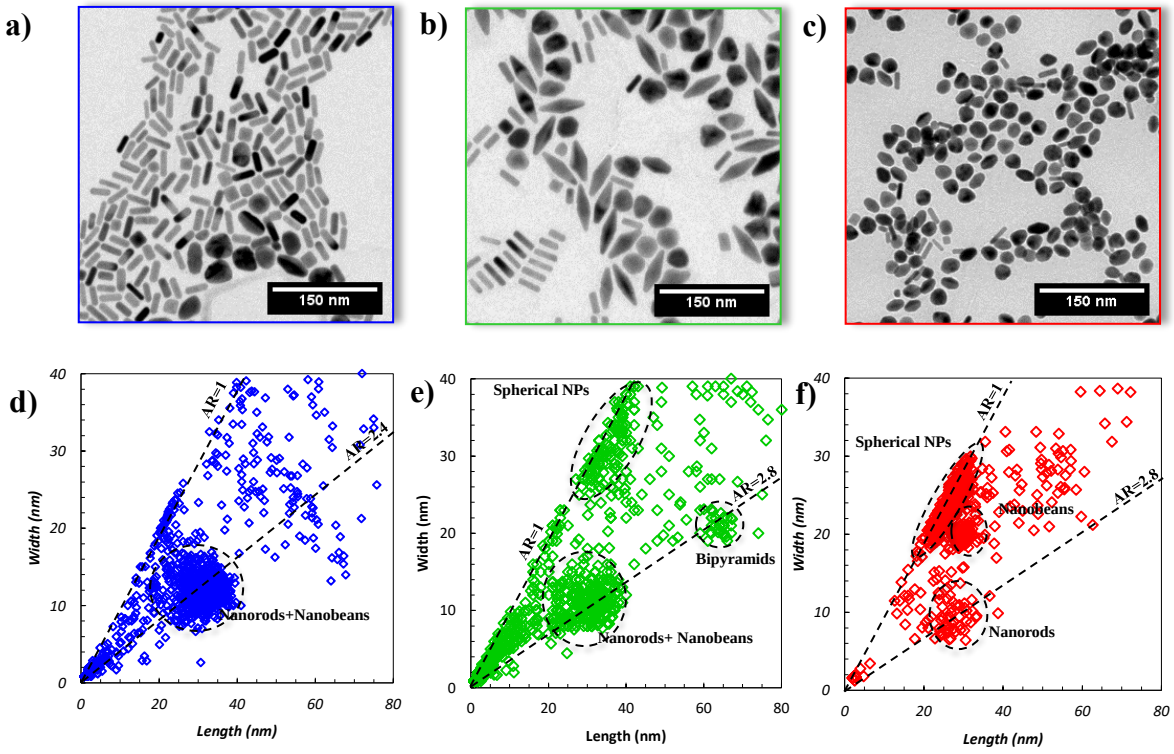


Figure 8. (Top) TEM images of samples obtained by competitive approach for different volumes of Type I and Type II seeds a) 100µL-20µL b) 60µL-60µL c) 96µL-192µL (see table 4 for

details). (Bottom) Size analysis on sample obtained from TEM data a) S1-99% Type I-1% Type II in numbers b) S2-93.8% Type I-6.2% Type II in numbers c) S3-88.5% Type I-11.5% Type II in numbers.

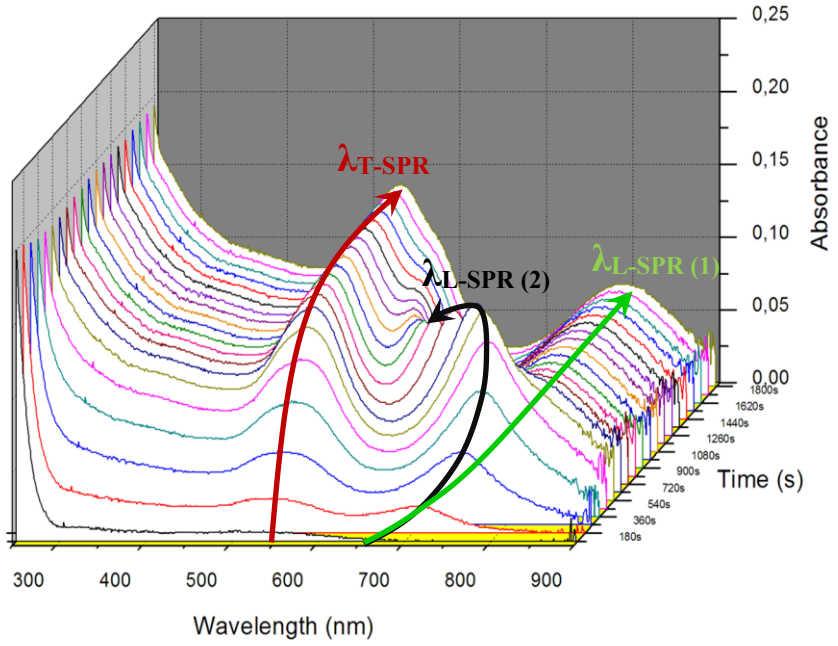


Figure 9. Time resolved UV-Vis Spectra of gold NP growth obtained via simultaneous addition of two different types of seeds in growth solution composed of 0.1 M CTAB, 0.5 mM $HAuCl_4$, 0.045 mM $AgNO_3$ and 0.75 mM L-Ascorbic Acid

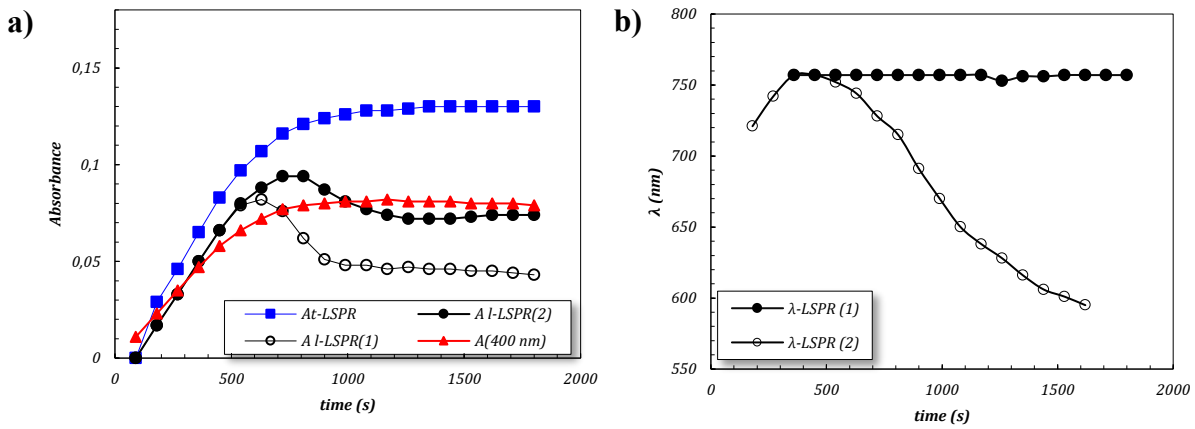


Figure 10. Relationship between a) absorbance's at 400 nm, transversal and longitudinal plasmon peaks b) maximum L-SPR values for nanorods (1) and nanobeans (2)

TABLES

Table 1. Synthetic conditions for the reference growth solution

Stock Solutions	**Quantity (mL)**	**[C_{final}] (mM)**
0.05M $HAuCl_4 \cdot 3H_2O$	0.1	0.5
0.1 M CTAB bromide)	10	98
0.01 M $AgNO_3$	0.045	0.045
0.1 M Ascorbic Acid	0.075	0.75

Table 2. Total number of particles and radius obtained by SAXS

Type of seed	**Type I**	**Type II**
Number density N_d (part/cm^3)	4.6 10^{14}	2.9 10^{13}
Radius <r> (nm)	1.00	2.40
Relative polydispersity σ/<r>	0.20	0.37

Table 3. Number and total specific surface in a given volume of added seeds of the two different seeds families.

Seed	d (nm) from SAXS	V_{seed} (µL)	N_{seed}	Σ (nm^2)
Type I	2.0	120	$5.5\ 10^{13}$	$6.9\ 10^{14}$
Type II	4.8	60	$1.8\ 10^{12}$	$1.3\ 10^{14}$

Table 4. Comparison of different experimental conditions with respect to added seed volume, number of seeds in corresponding volume and the surface area for the two kinds of seeds Type I seed and Type II seeds.

Sample Code	V_1 [(1)] µL	N_1 [(2)] (x10^{13})	V_2 [(1)] µL	N_2 [(2)] (x10^{12})	(%) N_1 [(4)]	(%) N_2 [(4)]	N1/N2	Σ_1[(5)](nm^2) (x10^{14})	Σ_2[(5)](nm^2) (x10^{14})	% Σ_1[(6)]	% Σ_1[(6)]
S1	100	4.6	20	0.6	98.7	1.3	76.7	5.8	0.45	92.7	8.3
S2	60	2.8	60	1.8	93.8	6.2	15.5	3.5	1.36	71.9	28.1
S3	96	4.4	192	5.8	88.5	11.5	7.6	5.5	4.3	56.1	43.9

[(1)] V_α = Volume of seed injected
[(2)] N_α = Number of seed in injected volume (V_α)
[(3)] N_T = Total number of seeds in overall volume ($V_1 + V_2$)
[(4)] $\%N_\alpha$ = Number percentage
[(5)] Σ_α= Surface area of seeds
[(6)] $\%\Sigma_\alpha$= Surface area percentage

ASSOCIATED CONTENT

Supporting Information

The Supporting Information is available free of charge at the XXXX website at DOI XXX.

AUTHOR INFORMATION

Corresponding Author

fabienne.testard@cea.fr

Author Contributions

The manuscript was written through contributions of all authors. All authors have given approval to the final version of the manuscript.

Notes

The authors declare no competing financial interests.

ACKNOWLEDGMENT

The authors acknowledge the French CNRS (Centre National de la Recherche Scientifique) (Grant FR3507) and CEA (Commissariat à l'Energie Atomique et aux Energies Alternatives) METSA (Microscopie Electronique et Sonde Atomique) network. The authors acknowledge the financial support from Agence Nationale de la Recherche (ANR) under Contract ANR-11_BS10_006. This work has been supported by the Region Ile-de-France in the framework of DIM C'Nano IdF.

ABBREVIATIONS

UV-Vis, UV Visible Spectroscopy; SAXS, Small Angle X-Ray Scattering; TEM, Transmission Electron Microscopy; DLS, Dynamic Light Scattering; FFT, Fast Fourier Transformation; Bipy, Bipyramid

REFERENCES

(1) Maltzahn, G.; Park, J.; Agrawal, A.; Bandaru, N. K.; Das, S. K.;Sailor, M. J.; Bhatia, S. N. Computationally Guided Photothermal Tumor Therapy Using Long-Circulating Gold Nanorod Antennas. *Cancer Res.* **2009**, *69*, 3982–3900.

(2) Gui, C.; Cui, D. Functionalized Gold Nanorods for Tumor Imaging and Targeted Therapy. *Cancer Biology & Medicine* **2012**, *9*, 221–233.

(3) Huang, X.; El-Sayed, M. A. Gold Nanoparticles: Optical Properties and Implementations in Cancer Diagnosis and Photothermal Therapy. *Journal of Advanced Research* **2010**, *1*, 13–28.

(4) Wei, A.; Leonov, A. P.; Wei, Q. Gold Nanorods: Multifunctional Agents for Cancer Imaging and Therapy. *Cancer Nanotechnology* **2010**, *624*, 119–130.

(5) Sengani, M.; Grumezescu, A. M.; Rajeswari, V. D. Recent Trends and Methodologies in Gold Nanoparticle Synthesis – A Prospective Review on Drug Delivery Aspect. *OpenNano* **2017**, *2*, 37–46. (6) Riley, R. S.; Day, E. S. Gold Nanoparticle-Mediated Photothermal Therapy: Applications and Opportunities for Multimodal Cancer Treatment. *Wiley Interdisciplinary Reviews: Nanomedicine and Nanobiotechnology* **2017**, *9*, e1449.

(7) Grzelczak, M.; Perez-Juste, J.; Mulvaney, P.; Liz-Marzan, L. M. Shape Control in Gold Nanoparticle Synthesis. *Chem. Soc. Rev.* **2008**, *37*, 1783–1791. (8) Burda, C.; Chen, X.; Narayanan, R.; El-Sayed, M. A. Chemistry and Properties of Nanocrystals of Different Shapes. *Chem. Rev.* **2005**, *105*, 1025–1102.

(9) Pérez-Juste, J.; Pastoriza-Santos, I.; Liz-Marzán, L. M.; Mulvaney, P. Gold Nanorods: Synthesis, Characterization and Applications. *Coordination Chemistry Reviews* **2005**, *249*, 1870–1901.

(10) Lohse, S. E.; Murphy, C. J. The Quest for Shape Control: A History of Gold Nanorod Synthesis. *Chem. Mater.* **2013**, *25*, 1250–1261.

(11) A. Gole and C. J. Murphy. Seed-Mediated Synthesis of Gold Nanorods: Role of the Size and Nature of the Seed. *Chem. Mater.* **2004**, *16*, 3633–3640.

(12) Murphy, C. J.; Sau, T. K.; Gole, A. M.; Orendorff, C. J.; Gao, J.; Gou, L.; Hunyadi, S. E.; Li, T. Anisotropic Metal Nanoparticles: Synthesis, Assembly, and Optical Applications. *J. Phys. Chem. B* **2005**, *109*, 13857–13870.

(13) Rodríguez-Fernández, J.; Pérez-Juste, J.; Mulvaney, P.; Liz-Marzán, L. M. Spatially-Directed Oxidation of Gold Nanoparticles by Au(III)−CTAB Complexes. *J. Phys. Chem. B* **2005**, *109*, 14257–14261.

(14) Scarabelli, L.; Sánchez-Iglesias, A.; Pérez-Juste, J.; Liz-Marzán, L. M. A "Tips and Tricks" Practical Guide to the Synthesis of Gold Nanorods. *J. Phys. Chem. Lett.* **2015**, *6*, 4270–4279.
(15) Burrows, N. D.; Vartanian, A. M.; Abadeer, N. S.; Grzincic, E. M.; Jacob, L. M.; Lin, W.; Li, J.; Dennison, J. M.; Hinman, J. G.; Murphy, C. J. Anisotropic Nanoparticles and Anisotropic Surface Chemistry. *J. Phys. Chem. Lett.* **2016**, *7*, 632–641.
(16) Liz-Marzán, L. M.; Grzelczak, M. Growing Anisotropic Crystals at the Nanoscale. *Science* **2017**, *356*, 1120.
(17) Wang, Z. L.; Mohamed, M. B.; Link, S.; El-Sayed, M. A. Crystallographic Facets and Shapes of Gold Nanorods of Different Aspect Ratios. *Surface Science* **1999**, *440*, L809–L814.
(18) Burrows, N. D.; Harvey, S.; Idesis, F. A.; Murphy, C. J. Understanding the Seed-Mediated Growth of Gold Nanorods through a Fractional Factorial Design of Experiments. *Langmuir* **2017**, *33*, 1891–1907.
(19) Gómez-Graña, S.; Hubert, F.; Testard, F.; Guerrero-Martínez, A.; Grillo, I.; Liz-Marzán, L. M.; Spalla, O. Surfactant (Bi)Layers on Gold Nanorods. *Langmuir* **2012**, *28*, 1453–1459.
(20) Chen, Y.; Fan, Z.; Zhang, Z.; Niu, W.; Li, C.; Yang, N.; Chen, B.; Zhang, H. Two-Dimensional Metal Nanomaterials: Synthesis, Properties, and Applications. *Chem. Rev.* **2018**, *118*, 6409–6455.
(21) Liu; Guyot-Sionnest, P. Mechanism of Silver(I)-Assisted Growth of Gold Nanorods and Bipyramids. *J. Phys. Chem. B* **2005**, *109*, 22192–22200.
(22) Hubert, F.; Testard, F.; Spalla, O. Cetyltrimethylammonium Bromide Silver Bromide Complex as the Capping Agent of Gold Nanorods. *Langmuir* **2008**, *24*, 9219–9222.
(23) Ghosh, S.; Manna, L. The Many "Facets" of Halide Ions in the Chemistry of Colloidal Inorganic Nanocrystals. *Chem. Rev.* **2018**, *118*, 7804–7864.
(24) Walsh, M. J.; Tong, W.; Katz-Boon, H.; Mulvaney, P.; Etheridge, J.; Funston, A. M. A Mechanism for Symmetry Breaking and Shape Control in Single-Crystal Gold Nanorods. *Acc. Chem. Res.* **2017**, *50*, 2925–2935.
(25) Niu, W.; Zhang, L.; Xu, G. Seed-Mediated Growth of Noble Metal Nanocrystals: Crystal Growth and Shape Control. *Nanoscale* **2013**, *5*, 3172–3181.
(26) Huang, X.; Neretina, S.; El-Sayed, M. A. Gold Nanorods: From Synthesis and Properties to Biological and Biomedical Applications. *Advanced Materials* **2009**, *21*, 4880–4910.
(27) Halder, A.; Kundu, P.; Viswanath, B.; Ravishankar, N. Symmetry and Shape Issues in Nanostructure Growth. *J. Mater. Chem.* **2010**, *20*, 4763–4772.
(28) Mariscal, M. M.; Velazquez-Salazar, J. J.; Yacaman, M. J. Growth Mechanism of Nanoparticles: Theoretical Calculations and Experimental Results. *CrystEngComm* **2012**, *14*, 544–549.
(29) C. J. Johnson, E. Dujardin, S. A. Davis, C. J. Murphy and S. Mann. Growth and Form of Gold Nanorods Prepared by Seed-Mediated, Surfactant-Directed Synthesis. *J. Mater. Chem.* **2002**, *12*, 1765–1770.
(30) Viswanath, B.; Kundu, P.; Halder, A.; Ravishankar, N. Mechanistic Aspects of Shape Selection and Symmetry Breaking during Nanostructure Growth by Wet Chemical Methods. *J. Phys. Chem. C* **2009**, *113*, 16866–16883.

(31) Hubert, F.; Testard, F.; Rizza, G.; Spalla, O. Nanorods versus Nanospheres: A Bifurcation Mechanism Revealed by Principal Component TEM Analysis. *Langmuir* **2010**, *26*, 6887–6891.
(32) Canbek, Z. C.; Cortes-Huerto, R.; Testard, F.; Spalla, O.; Moldovan, S.; Ersen, O.; Wisnet, A.; Wang, G.; Goniakowski, J.; Noguera, C.; et al. Twinned Gold Nanoparticles under Growth: Bipyramids Shape Controlled by Environment. *Crystal Growth & Design* **2015**, *15*, 3637–3644.
(33) Xia, Y.; Xiong, Y.; Lim, B.; Skrabalak, S. E. Shape-Controlled Synthesis of Metal Nanocrystals: Simple Chemistry Meets Complex Physics? *Angewandte Chemie International Edition* **2009**, *48*, 60–103.
(34) Nikoobakht, B.; El-Sayed, M. A. Preparation and Growth Mechanism of Gold Nanorods (NRs) Using Seed-Mediated Growth Method. *Chem. Mater.* **2003**, *15*, 1957–1962.
(35) Zemb, Th.; Taché, O.; Né, F.; Spalla, O. Improving Sensitivity of a Small Angle X-Ray Scattering Camera with Pinhole Collimation Using Separated Optical Elements. *Review of Scientific Instruments* **2003**, *74*, 2456–2462.
(36) Hubert, F.;Testard, F.; Thill, A.; Kong, Q.; Tache, O.; Spalla, O. Growth and Overgrowth of Concentrated Gold Nanorods: Time Resolved SAXS and XANES. *Cryst. Growth Des.* **2012**, *12*, 1548–1555.
(37) Kang, H.; Buchman, J. T.; Rodriguez, R. S.; Ring, H. L.; He, J.; Bantz, K. C.; Haynes, C. L. Stabilization of Silver and Gold Nanoparticles: Preservation and Improvement of Plasmonic Functionalities. *Chem. Rev.* **2019**, *119*, 664–699.
(38) Canbek, Z. C. Crystal Engineering of Anisotropic Gold Nanoparticles through Modulation of Seed Size and Crystal Structure, Universite de Versailles-Saint Quentin en Yvelines, 2014.
(39) Grzelczak, M.; Pérez-Juste, J.; Mulvaney, P.; Liz-Marzán, L. M. Shape Control in Gold Nanoparticle Synthesis. *Chem. Soc. Rev.* **2008**, *37*, 1783.
(40) Park, K.; Hsiao, M.-S.; Koerner, H.; Jawaid, A.; Che, J.; Vaia, R. A. Optimizing Seed Aging for Single Crystal Gold Nanorod Growth: The Critical Role of Gold Nanocluster Crystal Structure. *J. Phys. Chem. C* **2016**, *120*, 28235–28245.
(41) Wulff, G. Zeitschrift Fur Krishtallographie. *Zeitschrift fur Krishtallographie* **1901**, 449–530.
(42) Elechiguerra, J. L.; Reyes-Gasga, J.; Yacaman, M. J. The Role of Twinning in Shape Evolution of Anisotropic Noble Metal Nanostructures. *J. Mater. Chem.* **2006**, *16*, 3906–3919.
(43) Cortes-Huerto, R.; Goniakowski, J.; Noguera, C. Role of the Environment in the Stability of Anisotropic Gold Particles. *Phys. Chem. Chem. Phys.* **2015**, *17* (9), 6305–6313.
(44) Gulati, A.; Liao, H.; Hafner, J. H. Monitoring Gold Nanorod Synthesis by Localized Surface Plasmon Resonance. *J. Phys. Chem. B* **2006**, *110*, 22323–22327.
(45) Hendel, T.; Wuithschick, M.; Kettemann, F.; Birnbaum, A.; Rademann, K.; Polte, J. In Situ Determination of Colloidal Gold Concentrations with UV–Vis Spectroscopy: Limitations and Perspectives. *Anal. Chem.* **2014**, *86*, 11115–11124.
(46) Brioude, A.; Jiang, X. C.; Pileni, M. P. Optical Properties of Gold Nanorods: DDA Simulations Supported by Experiments. *J. Phys. Chem. B* **2005**, *109*, 13138–13142.
(47) Omi, H. Determination of Aspect-Ratio Distribution in Gold Nanowires Using Absorption Spectra and Transmission Electron Microscopy Techniques. In *The Transmission Electron Microscope*; InTech, 2012.

(48) Link, S.; El-Sayed, M. A. Simulation of the Optical Absorption Spectra of Gold Nanorods as a Function of Their Aspect Ratio and the Effect of the Medium Dielectric Constant. *J. Phys. Chem. B* **2005**, *109*, 10531–10532.
(49) Jana, N. R.; Gearheart, L.; Murphy, C. J. Seed-Mediated Growth Approach for Shape-Controlled Synthesis of Spheroidal and Rod-like Gold Nanoparticles Using a Surfactant Template. *Adv. Mater.* **2001**, *13*, 1389–1393.
(50) Lofton, C.; Sigmund, W. Mechanisms Controlling Crystal Habits of Gold and Silver Colloids. *Adv. Funct. Mater.* **2005**, *15*, 1197–1208.
(51) Bullen, C.; Zijlstra, P.; Bakker, E.; Gu, M.; Raston, C. Chemical Kinetics of Gold Nanorod Growth in Aqueous CTAB Solutions. *Crystal Growth & Design* **2011**, *11*,
(52) Becker, J.; Trügler, A.; Jakab, A.; Hohenester, U.; Sönnichsen, C. The Optimal Aspect Ratio of Gold Nanorods for Plasmonic Bio-Sensing. *Plasmonics* **2010**, *5*, 161–167.
(53) Zhao, Z.; Zheng, Z.; Roux, C.; Delmas, C.; Marty, J.-D.; Kahn, M. L.; Mingotaud, C. Importance of the Correlation between Width and Length in the Shape Analysis of Nanorods: Use of a 2D Size Plot To Probe Such a Correlation. *Chemistry – A European Journal* **2016**, *22*, 12424–12429.
(54) Lee, J.-H.; Gibson, K. J.; Chen, G.; Weizmann, Y. Bipyramid-Templated Synthesis of Monodisperse Anisotropic Gold Nanocrystals. *Nature Communications* **2015**, *6*, 7571.
(55) Wiley, B.; Herricks, T.; Sun, Y.; Xia, Y. Polyol Synthesis of Silver Nanoparticles: Use of Chloride and Oxygen to Promote the Formation of Single-Crystal, Truncated Cubes and Tetrahedrons. *Nano Lett.* **2004**, *4*, 1733–1739.
(56) Fleury, B.; Cortes-Huerto, R.; Taché, O.; Testard, F.; Menguy, N.; Spalla, O. Gold Nanoparticle Internal Structure and Symmetry Probed by Unified Small-Angle X-Ray Scattering and X-Ray Diffraction Coupled with Molecular Dynamics Analysis. *Nano Lett.* **2015**, *15*, 6088–6094.

TOC Graphic

